land

MDPI

Article

Land-Use-Change-Driven Erosion and Sediment Transport in the Yaqui River Sub-Basin (Mexico): Insights from Satellite Imagery and Hydraulic Simulations

Omar Salvador Areu-Rangel [1], Miguel Ángel Hernández-Hernández [2] and Rosanna Bonasia [3,*]

[1] Institute of Basic Sciences and Engineering, Universidad Autónoma del Estado de Hidalgo, Carretera Pachuca-Tulancingo Km. 4.5, Col. Carboneras, Mineral de la Reforma 42184, Mexico; omar_areu@uaeh.edu.mx
[2] Faculty of Engineering, Universidad Nacional Autónoma de México, Av. Universidad 3004, Copilco Universidad, Coyoacán, Ciudad de México 04510, Mexico; hbkmiguel458@outlook.com
[3] School of Engineering and Sciences, Tecnologico de Monterrey, Carretera Lago de Guadalupe Km 3.5 Atizapán de Zaragoza Col. Margarita Maza de Juarez, Cd López Mateos 52926, Mexico
* Correspondence: rosanna.bonasia@tec.mx

Abstract: Soil erosion and sediment transport are significant concerns in the Yaqui River sub-basin in northwest Mexico, driven by land use changes and environmental degradation. This study aims to evaluate erosion processes between 2000 and 2020 using a combination of satellite imagery and numerical simulations with Iber software (Version 2.5.2). The primary objective is to assess the impacts of land use changes, particularly the conversion of forest to grassland, on erosion rates and sediment transport. Satellite images from 2000 and 2020 were analyzed to detect land cover changes, while Iber's sediment transport module was used to simulate erosion patterns based on the Meyer–Peter and Müller equation for bedload transport. Hydrological and topographical data were incorporated to provide accurate simulations of flow velocity, depth, and erosion potential. The results reveal a 35.3% reduction in forest cover, leading to increased erosion and sediment transport in steep areas. Simulation predictions highlighted areas with high future erosion potential, which are at risk of further soil loss if current trends continue. Flow velocity increased, contributing to riverbank destabilization and higher sediment yield, posing a risk to infrastructure such as the Álvaro Obregón Dam. This study underscores the need for targeted erosion control measures and sustainable land management practices to mitigate future risks and protect vital infrastructure in the Yaqui River Basin.

Keywords: sediment transport processes; hydraulic simulations; soil recovery

check for updates

Citation: Areu-Rangel, O.S.; Hernández-Hernández, M.Á.; Bonasia, R. Land-Use-Change-Driven Erosion and Sediment Transport in the Yaqui River Sub-Basin (Mexico): Insights from Satellite Imagery and Hydraulic Simulations. *Land* **2024**, *13*, 1846. https://doi.org/10.3390/land13111846

Academic Editors: Jianjun Cao, Asim Biswas, Jian Zhang and Dewei Yang

Received: 28 September 2024
Revised: 31 October 2024
Accepted: 5 November 2024
Published: 6 November 2024

Copyright: © 2024 by the authors. Licensee MDPI, Basel, Switzerland. This article is an open access article distributed under the terms and conditions of the Creative Commons Attribution (CC BY) license (https://creativecommons.org/licenses/by/4.0/).

1. Introduction

Soil erosion and degradation significantly impact the environment, influencing physical, chemical, and biological processes [1–3]. Research has focused on the mechanical aspects of erosion, such as rainfall impact and surface runoff [4–6], as well as chemical factors like soil chemistry and salinity, and biological factors such as vegetation cover and land use changes [7–9]. These elements interact to influence the rates and patterns of soil erosion, particularly in regions where human activities such as deforestation and intensive agriculture exacerbate natural erosion processes. Methods such as field experiments, modeling, and remote sensing have shown that soil erosion affects agricultural productivity, contributes to sedimentation, reduces soil fertility, and disrupts natural habitats [10–14].

Physical factors, including rainfall intensity, wind velocity, and topography, are primary drivers of soil erosion [15–17]. Rainfall on steep slopes leads to surface runoff, detachment of soil particles, and sediment transport. Chemical factors, such as soil pH, salinity, and organic matter, affect soil cohesion and structure, altering its susceptibility to erosion [18,19]. Vegetation cover plays a critical role in preventing erosion by stabilizing

soil and reducing the impact of raindrops on the surface [20,21]. Land use changes, such as the conversion of forests to grasslands, can increase erosion risks by altering hydraulic parameters, reducing infiltration, and accelerating runoff.

The consequences of soil erosion extend beyond environmental degradation to include economic and social impacts [22]. Direct consequences include the loss of nutrient-rich topsoil, reduced agricultural productivity, sedimentation in water bodies, and damage to aquatic habitats. Indirect effects can include increased costs for infrastructure repairs, decreased carbon sequestration, and threats to food security in regions vulnerable to land degradation.

Traditionally, soil erosion and sediment transport have been assessed using field measurements like erosion pins and sediment traps, as well as empirical models such as the Universal Soil Loss Equation (USLE) and its revised version (RUSLE) [23,24]. While widely used, these methods have limitations, particularly in large or complex landscapes where processes such as sediment detachment, transport, and deposition interact in nonlinear ways. Recent advancements in technology have enhanced erosion assessments by incorporating remote sensing, GIS, and advanced hydrological models such as SWAT, HEC-RAS, and WEPP [25–27]. These models enable large-scale monitoring, simulate hydrological processes, and provide insights into erosion mechanisms.

The objective of this study is to evaluate water erosion in a sub-basin of the Yaqui River (state of Sonora, northwest Mexico) using satellite imagery and numerical simulations to assess the impact of land use changes on sediment transport from 2000 to 2020. The hydrodynamic simulations, conducted with Iber software [28], specifically target bedload transport and aim to provide insights into the morphological evolution of the sub-basin. This comprehensive approach aims to enhance the accuracy of erosion assessments and facilitate the development of targeted erosion control and soil recovery measures, providing valuable insights for environmental management. It is important to distinguish between the different erosion processes that occur on hillslopes and within river systems. Soil loss on hillslopes is often driven by processes such as raindrop impact, surface flow detachment, and the balance between erosion and sedimentation. In contrast, sediment transport in river systems typically involves distinct hydraulic conditions, including both bedload and suspended load transport. Suspended sediment transport is more characteristic of large, ancient rivers with low slopes, where it often dominates over bedload transport. However, the intermittent currents generated by short-duration rains and the steep slopes that define the hydrodynamics of the area make bedload transport the dominant process, while suspended sediment transport plays a secondary role. Given these specific hydrodynamic conditions, focusing on bedload transport is crucial for understanding sediment dynamics in this region.

2. Materials and Methods

2.1. Study Area Description

The state of Sonora is severely impacted by desertification, leading to intense soil degradation [29]. The Yaqui basin faces challenges such as water scarcity, competition for water resources, and environmental degradation [30–32]. Soil degradation and erosion are significant concerns in the basin, driven by intensive agricultural practices, deforestation, and overgrazing. The removal of vegetation cover, combined with the region's semi-arid conditions, accelerates soil erosion, resulting in the loss of topsoil and reduced agricultural productivity. Erosion also leads to sedimentation in the river and reservoirs, negatively affecting water quality and storage capacity. The Yaqui River Basin [33] spans across the states of Sonora and Chihuahua (Figure 1).

The basin covers approximately 72,000 km^2, with a main channel length of 27.44 km, an average slope of 1.11%, and a concentration time of 284 min, making it one of the region's most significant river basins. Located within the Río Yaqui-P. Álvaro Obregón sub-watershed in Hydrological Region 9, "Southern Sonora" [34], the Yaqui River originates in the Sierra Madre Occidental and flows southward for about 320 km before reaching

the Gulf of California. The basin features a semi-arid climate with significant variations in annual precipitation, with more rainfall in the mountainous upper regions and less in the lower, coastal areas. This precipitation variation, along with the river's flow regime, plays a crucial role in regional hydrology and water availability. Agriculture, particularly irrigated farming in the Yaqui Valley, dominates the basin's activities. Extensive irrigation infrastructure, including major dams like the Álvaro Obregón Dam (Figure 1), supports agriculture, flood control, hydroelectric power generation, and water supply for domestic and industrial use.

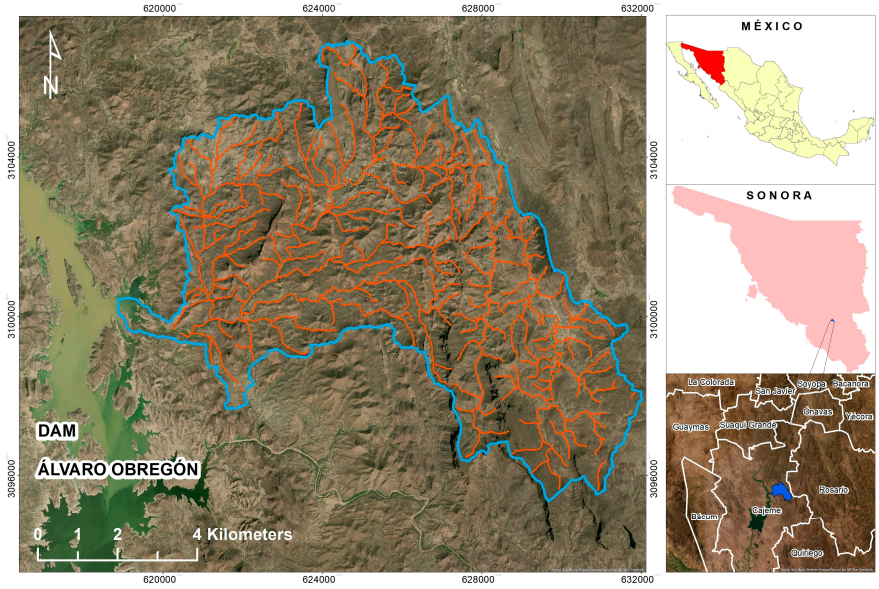


Figure 1. Location map of the Yaqui River basin in the state of Sonora.

Figure 2 shows the land use and lithology features of the study region, based on data reported by the National Commission for the Knowledge and Use of Biodiversity [35].

The land use map indicates that the predominant land use category is deciduous forest, which covers most of the basin, signifying a significant presence of seasonally shedding forested areas. There are also notable patches of cultivated grassland, particularly in the northern and southern parts of the basin, reflecting agricultural activities and land conversion for crop production. Smaller sections of induced grassland, where natural vegetation has been replaced or altered, suggest areas where natural grasslands have been altered by human intervention or secondary growth following deforestation or other disturbances. Additionally, lower thorny deciduous forest is present in some areas, indicating regions with vegetation adapted to drier conditions. Scattered throughout the basin are secondary vegetation, shrubs of low forest, and spine deciduous areas, which reflect mixed vegetation types, often indicative of transitional zones or regions recovering from past land use changes. The lithological map shows that andesite and andesitic tuff, found predominantly in the central and northern parts of the basin, indicate volcanic activity with intermediate volcanic rock and consolidated volcanic ash. The basalt-andesite lithology in the western and southwestern areas reflects a transition from mafic to intermediate volcanic compositions. Smaller patches of granite and granodiorite suggest ancient tectonic activity, while ignimbrite-rhyolitic tuff in the eastern region points to explosive volcanic events. Polygeneic conglomerate and conglomerate sandstone in various sections indicate past sedimentary processes. The combination of land use and lithological features suggests that areas with cultivated and induced grassland, as well as regions with volcanic and sedimentary rock types, may have higher soil erosion potential. The central and northern areas, with andesite and andesitic tuff, may face moderate to high erosion potential, especially where the rocks are weathered or fractured, and similar erosion risks are present in the basalt-andesite regions of the west and southwest.

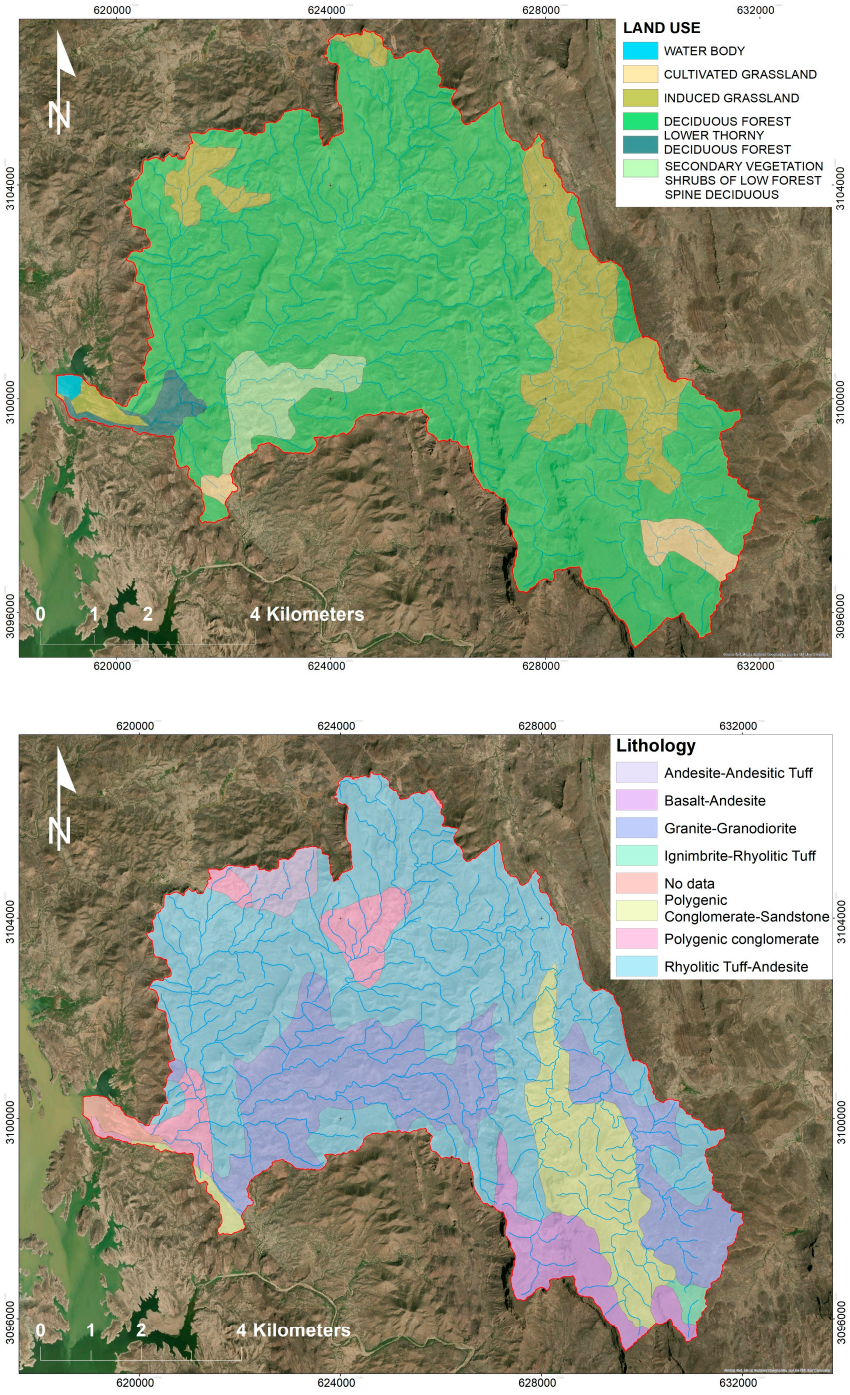


Figure 2. Land use and lithological characteristics maps of the study area [35]. The lithology map corresponds to 2019, and the land use map corresponds to 2021.

The Yaqui River Basin's fluvial network is primarily shaped by its semi-arid conditions and mountainous terrain. The network consists of ephemeral streams in the upper basin that are active during periods of intense rainfall, with a more defined river system in the lower basin. However, there is limited availability of gauging stations throughout the region, which restricts the direct observation of flow data. Additionally, there are no weather stations currently established in this portion of the basin to provide real-time distributed rainfall data.

In terms of erosive processes, the most dominant forms of erosion observed in the region are sheet and rill erosion, which occur across the slopes of the upper basin, where the vegetation cover has been removed or disturbed. Gully erosion may be observed,

particularly in areas with induced grassland and agricultural conversions. These gullies exacerbate soil loss, contributing significantly to the sediment load in the river, leading to sedimentation in downstream reservoirs and very low slope plains. Due to the combination of deforestation, agricultural expansion, and overgrazing, these processes pose a substantial risk to the region's topsoil, further intensifying the challenge of soil degradation.

2.2. Satellite Imagery to Analyze Soil Types

The land use analysis of the study area for the two selected scenarios (2000 and 2020) was conducted using the Corine Land Cover (CLC) database [36]. The CLC database, established in 1985 by the European Union, serves as a detailed and standardized inventory of land use and land cover across European countries, updated every six years. It classifies land cover into various categories, including natural and artificial landscapes, agricultural areas, forests, water bodies, and urban areas, making it a valuable tool for environmental analysis, urban planning, resource management, and assessing the impacts of human activities on the environment. Although originally developed for European regions, we used the CLC classification system as a reference framework in this study to ensure consistency and comparability in the land cover categories identified from satellite imagery. Its use allowed us to align land cover classes with a well-established framework and facilitated the identification of equivalent land cover types. The two scenarios selected in our analysis aim to capture significant land use changes over time, with satellite images from 2000 and 2020 providing high-quality data for observation and processing.

Land use scenarios for the years 2000 and 2020 were derived from satellite images acquired through the Google Earth portal [37], utilizing imagery from Landsat/Copernicus satellites. The highest available resolution and Reflective Color format images were used. To ensure seasonal consistency, we selected satellite images from December 2000 and January 2020, ensuring both datasets corresponded to the winter season, minimizing potential variations due to the presence of deciduous forest. Minimal cloud cover was also prioritized during the image selection process to improve the quality of land cover identification. These images were imported into ArcGIS software (Version 10.8) to identify land cover, with the Corine Land Cover database employed to ensure accurate classification and analysis. The software processed the images into a raster file containing 12 land use and vegetation classes, which were then homogenized to streamline the analysis. The output was converted into a text file format (ASCII) compatible with the Iber hydraulic model, facilitating the automatic assignment of roughness values and infiltration coefficients. The significance of these data in the hydraulic model will be discussed in the following paragraph.

Figure 3 illustrates the change in land use within the Yaqui basin from 2000 to 2020.

The upper images (a and b) display the original satellite images from the respective years, while the lower images (c and d) show the processed land use data. From 2000 to 2020, there is a noticeable increase in grassland areas (depicted in yellow) and a corresponding decrease in deciduous forest cover (depicted in green). The processed images indicate significant deforestation, with large patches of deciduous forest being converted to grassland. This change is particularly evident in the northern and central regions of the basin, where previously dense forest areas have been replaced by grassland. The expansion of grassland suggests increased agricultural activities or other land use changes that have led to the reduction of forested areas. The change in the reservoir's appearance between the two images in Figure 3 may reflect operational changes in the upstream reservoirs Angostura and Novillo, which impact the Álvaro Obregón reservoir. This change could indicate eutrophication processes caused by the accumulation of nutrients, such as nitrogen and phosphorus, from agricultural fertilizers or urban waste. As these processes do not follow seasonal cycles and occur downstream of the study basin, they were not included in the scope of this analysis. Figure 4 clearly shows how the land degradation process developed from 2000 to 2020, leading to a decrease in forest cover of 35.3%.

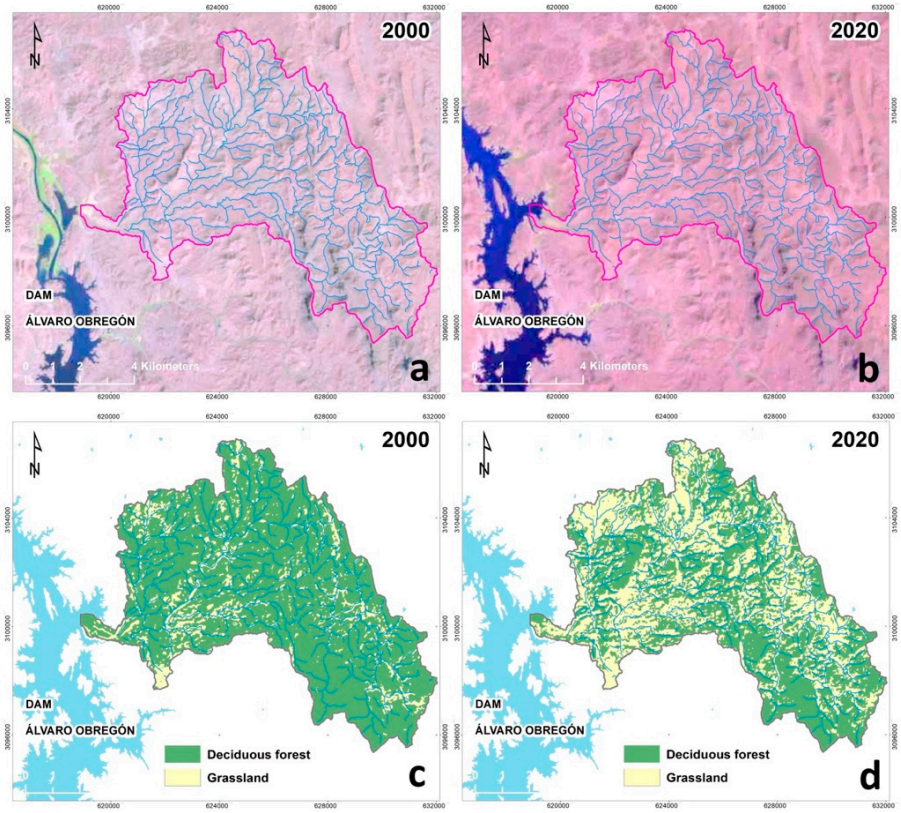


Figure 3. Result of the processing of satellite images of the study area. (**a**,**b**) Original satellite images corresponding to the 2000 and 2020 scenarios, respectively. (**c**,**d**) Land use maps obtained with image processing for the 2000 and 2020 scenarios, using the CLC database.

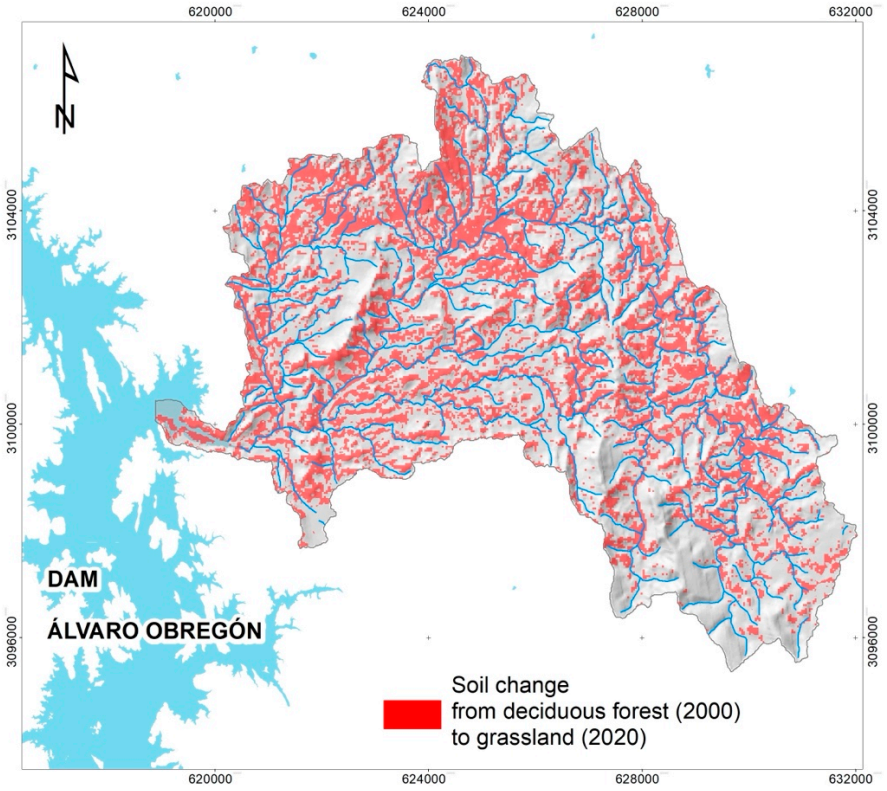


Figure 4. Map of soil evolution from 2000 to 2020, result of the analysis of satellite images. A decrease in forest cover of 35.3% is observed.

2.3. Numerical Simulations with Iber Software

In this study, we utilized the Iber software (Version 2.5.2) to simulate erosion and sediment transport. Iber is a two-dimensional, hydrodynamic modeling tool designed to simulate free-surface flow in rivers, estuaries, and coastal areas. It is widely used for flood hazard analysis, sediment transport, water quality studies, and environmental impact assessments. The Iber 2.5.2 version consists of several modules, including hydrodynamics, sediment transport, water quality, habitat modeling, and turbulence modeling. This modular structure allows users to perform integrated simulations tailored to their specific needs. The simulation process involved using Iber's sediment transport module, which solves the non-cohesive sediment transport equations for uniform grain sizes in a dynamic, non-stationary regime. We specifically selected the Meyer–Peter and Müller [38] equation, modified with the formulations of Wong [39], and Wong and Parker [40], for the calculation of the bedload:

$$q_{sb}^{*} = \mathbf{3.97}(\tau_{bs}^{*} - \tau_{c}^{*})^{\mathbf{3/2}} \quad (1)$$

where q_{sb}^{*} is the solid flow rate, τ_{bs}^{*} is the dimensionless grain stress, and τ_{c}^{*} is the dimensionless critical bed stress.

The Meyer–Peter and Müller equation is a classical formulation used to describe bedload transport, which refers to the movement of sediment particles along the riverbed. This equation is based on the concept of critical shear stress, which is the stress required to initiate sediment movement. The modifications introduced by Wong and Wong and Parker have enhanced the original equation by refining the criteria for sediment transport initiation and transport rate calculations, making it more accurate and applicable under a broader range of fluvial conditions. The implementation of this method within the Iber model, a widely validated tool for evaluating soil erosion processes, has been applied in several previous studies [41–44] to assess soil erosion at a seasonal scale, demonstrating the model's capability in distributed event-based erosion modeling, and in volcanic soil contexts, emphasizing its utility in managing erosion and flood risks in such complex settings.

In our simulations, we focused exclusively on bedload transport, deliberately neglecting suspended load transport. This decision was made because, in the context of our study, bedload transport exerts a significantly greater influence on sediment dynamics and erosion patterns compared to suspended load transport. While we acknowledge the potential for finer sediments, particularly on hillslopes, to be transported as suspended load, our focus on bedload transport in the channel system is grounded in the fact that bedload exerts a more significant influence on sediment dynamics and erosion patterns in the fluvial sections of the basin [45]. The hillslope contributions, where finer sediments may be mobilized, are likely to be less significant in the overall sediment budget, given the channel's ability to transport and deposit coarser materials. Furthermore, the hydrodynamic conditions in the main channel, with a high shear velocity, are more conducive to bedload transport, particularly during high-flow events [46]. Moreover, although we lack direct granulometric data for the study area, the lithological characteristics presented in Figure 2 provide valuable insights into the types of sediments likely present in the basin. The central and northern parts of the basin, predominantly composed of andesitic and volcanic tuff, suggest a landscape formed by intermediate volcanic rocks, which typically produce coarser sediments such as gravels and sands through weathering processes [47]. These materials are consistent with the types of sediments typically transported as bedload. In the western and southwestern areas, where basalt-andesite lithology is predominant, the presence of mafic to intermediate volcanic compositions further supports the likelihood of coarse sediment production, as these rock types tend to weather into larger fragments. By concentrating on bedload transport, we aimed to simplify the model without compromising the accuracy of the results, ensuring that the primary transport processes relevant to our specific study area are accurately represented.

To simulate the mechanism of erosion and sediment transport in this study, a digital elevation model created from the Mexican Elevation Continuous of the National Institute of Statistics and Geography [48] was used, with a resolution of 15 m. The computational

domain was discretized with an unstructured mesh of 115,441 elements, with elements of size 10 m for the steepest areas and 100 m in the rest of the calculation domain. The inlet flow imposed to initialize the water erosion process is 27 mm/h. This value was determined based on the morphological parameters of the basin, as detailed in Section 2.1. Due to the absence of distributed rainfall data, it was not possible to utilize precipitation data from local climatological stations, as no such stations are available in the study basin. The nearest climatological station, Nuri, is located in the municipality of Rosario, almost 40 km away, and belongs to a different sub-basin of the Yaqui River. For this reason, we relied on the isohyets provided by the Secretariat of Communications and Transport of Mexico [49], selecting a concentration time of 240 min, which is the closest approximation to the concentration time of the study basin. Additionally, a return period of 25 years was chosen, corresponding to the nearest period between the two scenarios considered. Surface roughness was characterized by assigning two Manning's coefficients: 0.12 for deciduous forest and 0.05 for grassland. The allocation of these coefficients was primarily based on the area's land use properties defined by means of the satellite images analysis described in Section 2.2 to distinguish more accurately between areas of varying erodibility. An initial water depth condition of zero was set for the domain. Table 1 displays the numerical parameters and sediment properties used for calculating bed shear stress and erosion.

Table 1. Numerical and sediment parameters for erosion/transport simulations.

Numerical and Sedimentological Parameters	Value
Max simulation time (s)	25,200
Numerical scheme	First Order
Grain diameter d50 (m)	0.00019
Friction angle	0.55
Bed porosity	2.65

The sedimentological characteristics of the study area, including the average diameter (d50) of soil particles, relative density (bed porosity), and internal friction angle, were derived from an environmental impact study conducted in the region, published by the Secretariat of the Environment and Natural Resources [50].

To account for infiltration losses, the Iber software provides the option to apply an infiltration model. In this study, the Curve Number model [51] from the Soil Conservation Service was utilized. The application of the Curve Number (CN) depends on the terrain slope, land use, soil type, and antecedent moisture conditions (AMC). In this study, under normal AMC conditions (AMC II), an average CN value of 77 was assigned for the year 2000 scenario and 80 for the year 2020 scenario. The assumption of AMC II was made to reflect possible moderate soil moisture levels after significant rainfall events. Land-use-change characteristics were assigned based on the results of the processing of satellite images in Figure 3. The CN value of 77 for 2000 corresponds to an area largely dominated by deciduous forest, where the soils fall under hydrologic soil group B, characterized by moderate infiltration. By 2020, an increased presence of grassland, combined with soil degradation, resulted in a CN value of 80, indicating a shift towards hydrologic soil group C, which is associated with lower infiltration rates. This increase in CN reflects a trend towards higher surface runoff due to the combined effects of soil compaction, vegetation loss, and reduced infiltration capacity.

The results of the simulations are calculated values of water depth and velocity, as well as erosion depths and sediment transport values.

3. Results

3.1. Flow Depth and Velocity

Figure 5 shows the results of the hydraulic simulations for the calculated values of flow depth (a and b) and velocity (c and d) for the two simulated scenarios (2000 and 2020).

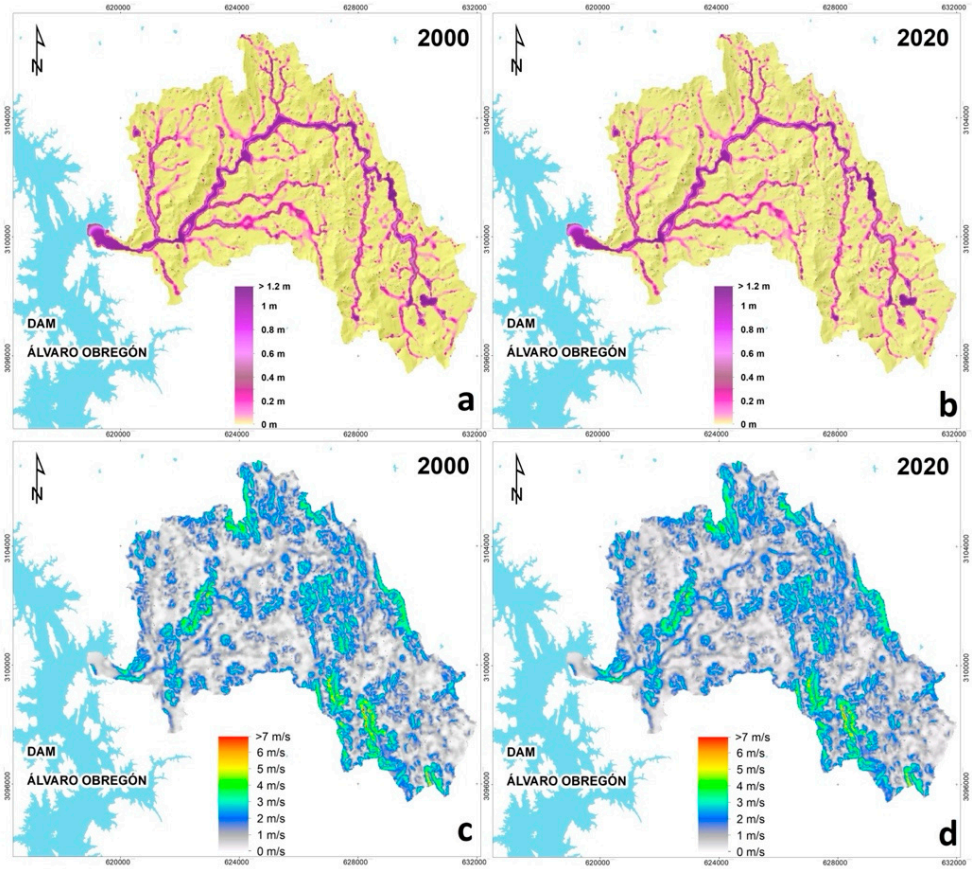


Figure 5. Results of hydraulic simulations. Flow depth: (**a**) 2000 scenario and (**b**) 2020 scenario. Flow velocity: (**c**) 2000 scenario and (**d**) 2020 scenario.

In the 2000 scenario, the water depth map shows a relatively moderate distribution of water depth across the study area, with depths ranging from 0 to over 1.2 m. The deeper regions are primarily located along the main river channels. In contrast, the 2020 scenario indicates a general decrease in water depth due to a reduction in vegetation cover. The lack of vegetation results in less flow resistance, allowing water to flow more freely and increasing overall flow velocity. However, there are areas where flow accumulates, leading to localized increases in water depth. It is important to note that the differences in depth values between the two scenarios are on the order of 10 cm. These subtle changes in depth can have impacts on erosion and sediment transport processes. The reduction in water depth combined with increased flow velocity can exacerbate the erosion of riverbanks and bed materials, contributing to channel instability and morphological changes. This suggests a complex interaction between flow dynamics and terrain features, where certain areas experience higher water depths despite the overall trend of reduced depth. The flow velocity maps, for the two scenarios, further illustrate these changes. In the 2000 scenario, flow velocities range from 0 to over 7 m/s, with higher velocities concentrated in narrower and steeper channels. The 2020 scenario also exhibits flow velocities up to over 7 m/s but shows a broader distribution of high-velocity areas. This overall increase in flow velocity is attributed to decreased vegetation cover, which reduces the natural resistance to flow and accelerates water movement across the landscape.

3.2. Erosion and Sedimentation Patterns

Figure 6 presents the results of the erosion and sediment transport simulations for the two scenarios: 2000 (a) and 2020 (b). Erosion values are represented in meters, with negative values indicating sediment deposition.

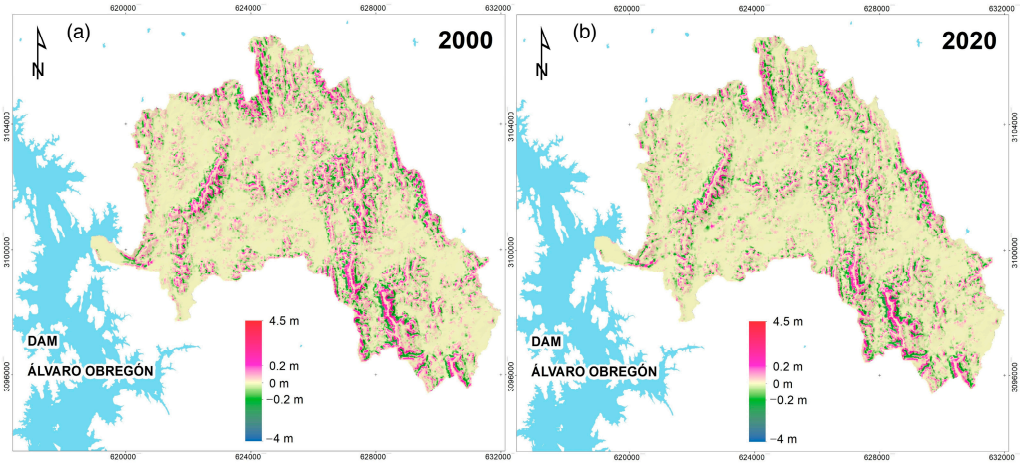


Figure 6. Results of sediment transport and erosion simulations: (**a**) 2000 scenario and (**b**) 2020 scenario.

In the 2000 scenario, erosion and deposition are widely distributed across the study area, with both erosion (positive values) and sediment deposition (negative values) occurring in various locations. The erosion values, represented in meters, range from −4 m (indicating sediment deposition) to 4.5 m (indicating erosion). Areas with greater erosion correspond to those with the highest flow speeds (shown in Figure 5), with higher velocities concentrated in narrower and steeper channels. In the 2020 scenario, the overall patterns of erosion and deposition remain similar, but there are changes in their intensity and distribution. The reduction in vegetation cover likely contributes to increased sediment mobility and altered flow dynamics. Consequently, there is a general increase in areas experiencing erosion, particularly along the riverbanks and regions with steep slopes. However, at the base of the mountainous area, sedimentation is observed due to the change in flow speed when the water reaches flatter areas, causing sediments to settle.

3.3. Impact Analysis

Figure 7 shows the areas where the change in land use from forest to grassland has been concentrated, depicted in light purple.

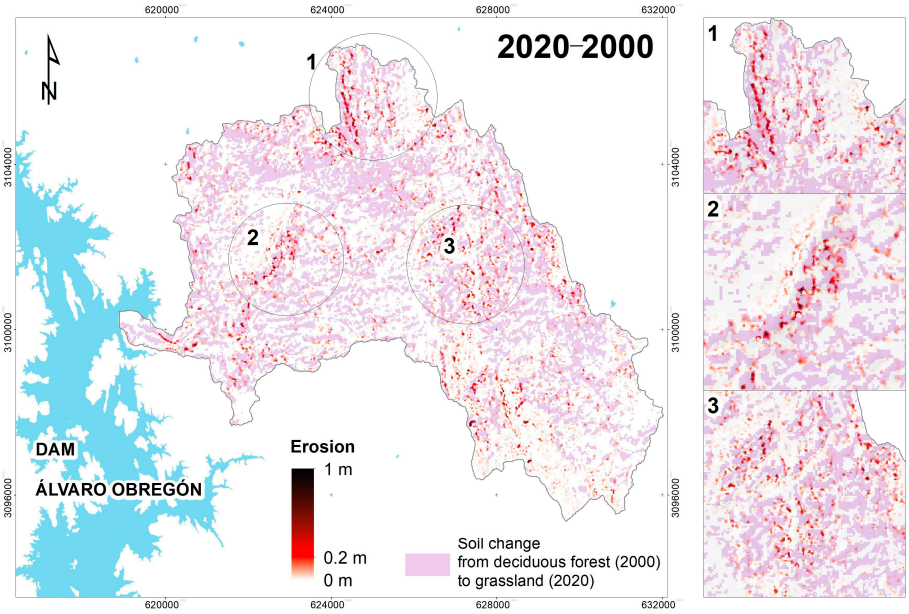


Figure 7. Comparison of erosion and land use change in the basin between 2000 and 2020. Light purple areas indicate land use change from deciduous forest to grassland. The highlighted zones (1, 2, and 3) show regions with notable erosion increase due to steep slopes and land use changes.

The figure also illustrates the difference in erosion depths between the two scenarios, highlighting how erosion has increased over the years. Erosion values are represented in meters, ranging from 0 to 1, with areas of significant erosion increase shown in darker shades.

The three highlighted zones (1, 2, and 3) indicate specific areas with notable changes. Zone 1, located in the northern part of the basin, shows a significant increase in erosion. The steep slopes in this region, combined with the change in land use from deciduous forest to grassland, have likely exacerbated soil erosion. The loss of forest cover reduces the soil's stability and increases its vulnerability to erosion by water runoff. Zone 2, in the central part of the basin, also exhibits high erosion rates. Similar to Zone 1, the conversion of forest to grassland has led to increased soil erosion. The central location within the basin means that erosion here can have downstream effects, contributing to sedimentation in lower-lying areas and potentially impacting water quality in connected water bodies. Zone 3, in the southern part of the basin, shows erosion increase concentrated along steep slopes. The land use change from forest to grassland has similarly contributed to this scenario.

Figure 8 illustrates erosion potential areas in the sub-basin, considering both the changes in land use from deciduous forest to grassland between 2000 and 2020 and eliminating the effect of erosion that already occurred during this period.

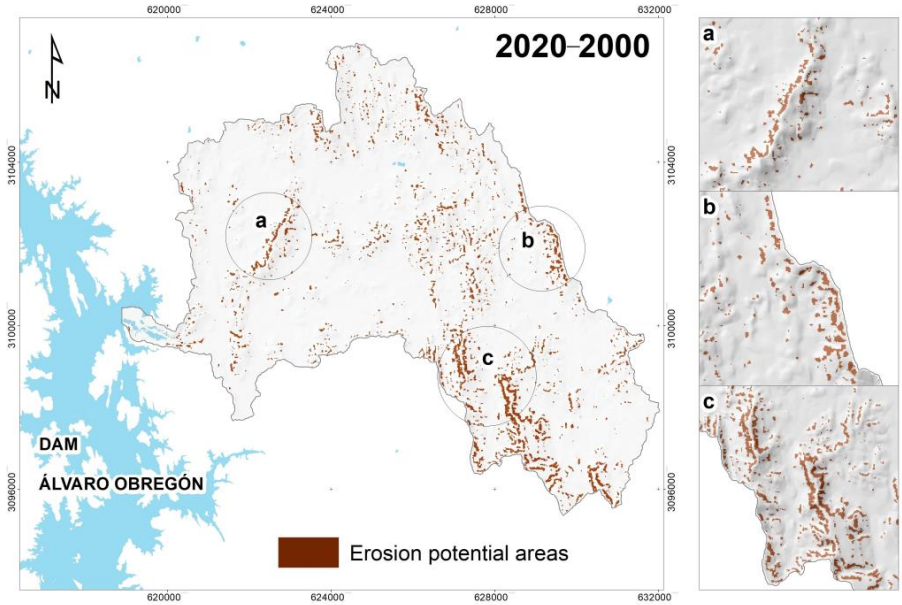


Figure 8. Erosion potential areas in a sub-basin of the Yaqui River, highlighting regions with high future erosion potential (marked as "a", "b", and "c") due to slopes and potential future soil degradation.

It is important to note that the areas where erosion potential zones are concentrated have not yet experienced significant soil degradation but represent regions at high risk of future soil loss. This assessment is based on the patterns observed between 2000 and 2020, where changes in land use—particularly the shift from deciduous forest to grassland—along with steep slopes and reduced vegetation cover, have increased the susceptibility to erosion. If these trends continue, these areas may experience progressive soil degradation, extending the impact of erosion beyond what has already occurred. The areas marked "a", "b", and "c" are highlighted for their high future erosion potential due to their slopes and possible soil degradation. Area "a" is located in the northwestern part of the sub-basin. This area shows a significant concentration of potential erosion zones, likely due to the combination of steep slopes and future soil degradation. Area "b" is situated in the central part of the sub-basin. The map highlights a dense pattern of erosion potential zones, indicating that this area is particularly vulnerable. The central location and specific topographic features contribute to the high erosion risk. Area "c" is found in the southeastern part of the sub-basin. Similar to areas "a" and "b", it exhibits a high concentration of erosion potential zones. The slopes and soil conditions in this area are conducive to significant soil loss, as depicted in the

inset detail for area "c". The erosion in these areas also has significant consequences for sediment transport in water bodies, particularly affecting the Álvaro Obregón Dam. This sediment is likely to be transported by surface runoff into nearby streams. The transport pathways from Area "a" to the dam are longer and involve multiple water bodies, which can lead to sediment deposition along the way, reducing the overall sediment load reaching the dam. Its central location of Area "b" means that sediment can be readily transported into major streams that flow toward the dam. This area is highly prone to contributing sediment to the dam due to its proximity and direct hydrological connections. Sediment from Area "c" is likely to be transported into streams and rivers that directly feed into the dam. Given its location and topography, Area "c" is the most prone to having its eroded sediment transported into the dam, posing a significant risk for increased sedimentation in the dam reservoir.

4. Discussion

The findings of this study have significant implications for erosion control and soil recovery measures. Results of the hydraulic simulations depicted in Figure 5 show that higher flow velocities in the 2020 scenario enhance the river's transport capacity, leading to increased sediment transport and potential deposition in downstream areas where flow velocity decreases. Additionally, the reduction in water depth combined with increased flow velocity can exacerbate the erosion of riverbanks and bed materials, contributing to channel instability and morphological changes. From the comparison of erosion and land use change in the basin between 2000 and 2020 (Figure 7), the impact of erosion on the basin's ecosystem is significant. Soil loss in these steep areas, exacerbated by the conversion of forests to grasslands, can lead to a decrease in the soil's ability to retain water and nutrients, negatively affecting local vegetation and reducing biodiversity. Erosion can also increase sedimentation in water bodies. These erosion patterns can have significant implications for the Álvaro Obregón Dam, as increased sediment transport can reduce the dam's capacity, impair its functionality, and degrade water quality. In terms of the area's morphology, accelerated erosion in steep regions can lead to the formation of gullies and ravines, significantly altering the landscape. These changes in topography can modify water flow patterns, increasing the risk of flooding in lower areas of the basin.

The identification of high erosion potential areas provides valuable information for targeted erosion control interventions. Area "c" in Figure 8, with its direct hydrological connection to the Álvaro Obregón Dam, is particularly prone to sediment transport, posing a significant risk for increased sedimentation in the dam reservoir. Effective erosion control in this area is crucial to maintaining the dam's capacity and functionality. The methodology applied in this study shows that the sediment generated from erosion can lead to siltation in the Álvaro Obregón Dam. This siltation can reduce the dam's storage capacity, affect water quality, and potentially increase the need for costly dredging operations.

The Yaqui River basin faces significant challenges with soil erosion and land degradation, which are worsening over time. Environmental studies and restoration efforts highlight concerns about erosion, water management, and degradation. The Green Revolution negatively impacted the basin, as export-focused agriculture led to pesticide overuse, groundwater depletion, and environmental harm, affecting water quality, local farming, and biodiversity [52–54]. Despite studies on the impact of the Novillo, Angostura, and Álvaro Obregón dams on water capacity [55], environmental and social issues persist. The Yaqui tribe's ongoing fight for water rights underscores the need for sustainable, inclusive water policies that honor indigenous rights and ensure fair resource distribution.

The methodology employed in this study, which combines satellite imagery analysis with advanced numerical simulations using the Iber software, has demonstrated effectiveness in assessing water erosion and sediment transport in the Yaqui River sub-basin. The use of high-resolution satellite images from Landsat/Copernicus satellites, coupled with a digital elevation model, enabled precise characterization of land cover changes and identification of potential erosion zones and provided insights into areas that have not yet

experienced significant soil degradation but may be at risk in the future. This approach offers several advantages over traditional methodologies. Field-based measurements, such as erosion pins, sediment traps, and runoff plots, while providing direct observations of soil loss and sediment deposition, are often labor-intensive and limited in spatial and temporal scope, with problems of scale dependency of erosion rates [56]. On the other hand, monitoring techniques for soil erosion face several limitations, particularly when compared to more controlled experimental approaches such as runoff plots. Field-based monitoring, which relies on surveys and mapping, often lacks the precision of plot studies. This approach generally assumes that splash and sheetwash are minor factors in soil redistribution, focusing instead on rills and gullies as the primary movers of soil within a field or landscape. The rate of erosion measured by the size of rills and gullies is influenced by the frequency and intensity of recent storm events so that temporal variations in rainfall further complicate the estimation of erosion rates from rill erosion [57].

While the approach proposed in this work has significant strengths, it is important to acknowledge certain uncertainties and limitations. The lack of direct granulometric data introduces uncertainty into the sediment transport model, especially in calculating bedload transport. Although lithological characteristics suggest the presence of coarse sediments, without measured grain-size distribution, the simulated transport rates may not fully capture sediment variability across the sub-basin. The absence of real-time precipitation data is another limitation. The use of isohyet maps and assumptions of uniform rainfall may not adequately reflect the spatial variability of precipitation in the region, affecting the accuracy of hydrodynamic simulations and their ability to capture localized runoff and erosion events. Additionally, while Iber effectively simulates bedload transport for coarse sediments, the decision to exclude suspended sediment transport means that finer-grained sediments, especially from hillslopes, may not be fully represented. This focus could lead to an underestimation of the total sediment load.

Despite the mentioned limitations, modern methodologies, like the one used in this study, leverage technological advances to improve erosion assessments. These tools are particularly useful in data-scarce regions, such as many micro-basins in Mexico, where field observations are limited. Remote sensing and GIS provide broad spatial coverage and temporal resolution, helping identify erosion hotspots and sediment pathways [58,59]. Hydrological and hydraulic models combine climatic, hydrological, and land use data to simulate water flow and sediment transport [60,61], accounting for spatial and temporal variability. Iber software plays a key role by simulating sediment transport and analyzing flow patterns like depth and velocity, which are crucial for understanding erosion.

This study highlights the need for soil conservation practices like reforestation, terracing, and controlled grazing to stabilize soil and reduce erosion risks. Targeted actions in high-risk areas can prevent degradation, sustain agricultural productivity, and protect water bodies from sedimentation. This study's predictive capabilities support proactive erosion control strategies, promoting sustainable land and water management. Policy recommendations include promoting conservation practices, particularly in high-risk areas, and implementing remote sensing and GIS-based monitoring programs to track land use changes and erosion patterns. Sustainable land management practices are essential to balance conservation with agricultural productivity. Guidelines for infrastructure development and maintenance should minimize erosion impacts and protect critical facilities like the Álvaro Obregón Dam.

Several recommendations can be made to improve the accuracy of future studies. First, the collection of field data, including granulometric measurements and real-time precipitation data, would provide valuable inputs for model calibration and validation. Incorporating suspended sediment transport into the modeling framework would also offer a more comprehensive understanding of sediment dynamics in the basin. Additionally, the use of more advanced infiltration models that account for spatial variability in soil properties and moisture conditions could enhance the accuracy of runoff and sediment transport predictions.

5. Conclusions

The Yaqui River basin is severely impacted by soil erosion and land degradation, driven by deforestation, agricultural expansion, and overgrazing, which threaten the region's agricultural productivity, water resources, and ecosystems. Using a combination of high-resolution satellite imagery and numerical simulations with the Iber software, this study assessed erosion processes and sediment transport patterns between 2000 and 2020. The results identified critical areas with increased erosion potential, particularly due to land use changes, such as the conversion of deciduous forest to grassland, leading to higher sediment transport toward key infrastructure like the Álvaro Obregón Dam.

The identification of erosion-prone areas provides valuable insights for targeted interventions. Specifically, areas at high risk of future erosion—identified through patterns observed over the past two decades—should be prioritized for soil conservation practices, such as reforestation, terracing, and controlled grazing. Implementing such measures will help stabilize the soil, reduce erosion risks, and prevent further sedimentation in key water bodies. The findings underscore the importance of integrated land and water management to maintain the region's agricultural productivity and ecosystem health.

Future studies could benefit from the collection of field data, including granulometric measurements and real-time precipitation data, to further refine hydrodynamic models and validate results. Additionally, expanding the modeling framework to include suspended sediment transport would provide a more comprehensive understanding of sediment dynamics, particularly for finer sediments transported from hillslopes. Incorporating advanced infiltration models would also enhance the accuracy of runoff and erosion predictions.

The approach applied in this study, despite limitations related to data availability, offers a scalable and practical solution for regions facing similar erosion challenges. The use of remote sensing, GIS, and numerical modeling provides a framework that can support policymakers and land managers in identifying erosion hotspots and designing sustainable interventions. Our findings emphasize the need for proactive erosion control strategies to preserve agricultural lands, protect vital infrastructure, and ensure long-term sustainability in the Yaqui River basin.

Author Contributions: Conceptualization, O.S.A.-R. and R.B.; methodology, O.S.A.-R. and M.Á.H.-H.; software, O.S.A.-R.; validation, O.S.A.-R. and R.B.; formal analysis, O.S.A.-R., M.Á.H.-H. and R.B.; investigation, O.S.A.-R., M.Á.H.-H. and R.B.; resources, O.S.A.-R.; data curation, O.S.A.-R. and R.B.; writing—original draft preparation, O.S.A.-R. and R.B.; writing—review and editing, O.S.A.-R., M.Á.H.-H. and R.B.; visualization, O.S.A.-R.; supervision, R.B.; project administration, R.B.; funding acquisition, R.B. All authors have read and agreed to the published version of the manuscript.

Funding: This research received no external funding.

Data Availability Statement: Data are contained within the article.

Conflicts of Interest: The authors declare no conflicts of interest.

References

1. Issaka, S.; Ashraf, M.A. Impact of soil erosion and degradation on water quality: A review. *Geol. Ecol. Landsc.* **2017**, *1*, 1–11. [CrossRef]
2. Steinhoff-Knopp, B.; Kuhn, T.K.; Burkhard, B. The impact of soil erosion on soil-related ecosystem services: Development and testing a scenario-based assessment approach. *Environ. Monit. Assess.* **2021**, *193*, 274. [CrossRef]
3. Hermassi, T.; Kotti, M.L.; Jarray, F. Soil Erosion in a Changing Environment over 40 Years in the Merguellil Catchment Area of Central Tunisia. *Appl. Sci.* **2023**, *13*, 11641. [CrossRef]
4. Chen, H.; Zhang, X.; Abla, M.; Lü, D.; Yan, R.; Ren, Q.; Ren, Z.; Yang, Y.; Zhao, W.; Lin, P.; et al. Effects of vegetation and rainfall types on surface runoff and soil erosion on steep slopes on the Loess Plateau, China. *CATENA* **2018**, *170*, 141–149. [CrossRef]
5. Fang, N.F.; Wang, L.; Shi, Z.H. Runoff and soil erosion of field plots in a subtropical mountainous region of China. *J. Hydrol.* **2017**, *552*, 387–395. [CrossRef]
6. Sun, T.; Deng, L.; Fei, K.; Fan, X.; Zhang, L.; Ni, L.; Sun, R. Runoff Characteristics and Soil Loss Mechanism in the Weathered Granite Area under Simulated Rainfall. *Water* **2021**, *13*, 3453. [CrossRef]
7. Smith, P.; House, J.I.; Bustamante, M.M.C.; Sobocká, J.; Harper, R.; Pan, G.; West, P.C.; Clark, J.M.; Adhya, T.; Rumpel, C.; et al. Global change pressures on soils from land use and management. *Glob. Change Biol.* **2015**, *22*, 1008–1028. [CrossRef]

8. Almohamad, H. Impact of Land Cover Change Due to Armed Conflicts on Soil Erosion in the Basin of the Northern Al-Kabeer River in Syria Using the RUSLE Model. *Water* **2020**, *12*, 3323. [CrossRef]
9. Roxo, M.J.; Cerqueira, H.M.; Calvo-Cases, A. The role of land use and land cover changes in triggeringsoil losses in the SE Alentejo, Portugal. *Land Degrad. Dev.* **2023**, *34*, 5954–5968. [CrossRef]
10. Pimentel, D. Soil Erosion and the Threat to Food Security and the Environment. *Ecosyst. Health* **2001**, *6*, 221–226. [CrossRef]
11. Wirtz, S.; Seeger, M.; Ries, J.B. Field experiments for understanding and quantification of rill erosion processes. *CATENA* **2012**, *91*, 21–34. [CrossRef]
12. Mitasova, H.; Barton, M.; Ullah, I.; Hofierka, J.; Harmon, R.S. 3.9 GIS-Based Soil Erosion Modeling. In *Treatise on Geomorphology*; Academic Press: Cambridge, MA, USA, 2013; pp. 228–258. [CrossRef]
13. Novara, A.; Pisciotta, A.; Minacapilli, M.; Maltese, A.; Capodici, F.; Cerdà, A.; Gristina, L. The impact of soil erosion on soil fertility and vine vigor. A multidisciplinary approach based on field, laboratory and remote sensing approaches. *Sci. Total Environ.* **2018**, *622–623*, 474–480. [CrossRef] [PubMed]
14. Xu, H.; Hu, X.; Guan, H.; Zhang, B.; Wang, M.; Chen, S.; Chen, M. A Remote Sensing Based Method to Detect Soil Erosion in Forests. *Remote Sens.* **2019**, *11*, 513. [CrossRef]
15. Guerra, C.A.; Rosa, I.M.D.; Valentini, E.; Wolf, F.; Filipponi, F.; Karger, D.N.; Xuan, A.N.; Mathieu, J.; Lavelle, P.; Eisenhauer, N. Global vulnerability of soil ecosystems to erosion. *Landsc. Ecol.* **2020**, *35*, 823–842. [CrossRef] [PubMed]
16. Wang, J.; Gong, Q.; Yu, Y. Assessing the Influence of Environmental Factors on Spatial Soil Erosion Risk based on the Certainty Coefficient Method. *J. Risk Anal. Crisis Response* **2021**, *8*, 131–141. [CrossRef]
17. Wen, L.; Peng, Y.; Zhou, Y.; Cai, G.; Lin, Y.; Li, B. Study on soil erosion and its driving factors from the perspective of landscape in Xiushui watershed, China. *Sci. Rep.* **2023**, *13*, 8182. [CrossRef] [PubMed]
18. Misra, R.K.; Teixeira, P.C. The sensitivity of erosion and erodibility of forest soils to structure and strength. *Soil Tillage Res.* **2001**, *59*, 81–93. [CrossRef]
19. Nunes, M.R.; da Silva, A.P.; Denardin, J.E.; Giarola, N.F.B.; Vaz, C.M.P.; van Es, H.M.; da Silva, A.R. Soil chemical management drives structural degradation of Oxisols under a no-till cropping system. *Soil Res.* **2017**, *55*, 819–831. [CrossRef]
20. Mahmoudzadeh, A. Vegetation cover plays the most important role in soil erosion control. *Pak. J. Biol. Sci.* **2007**, *10*, 388–392. [CrossRef]
21. Xiong, M.; Leng, G.; Tang, Q. Global Analysis of the Cover-Management Factor for Soil Erosion Modeling. *Remote Sens.* **2023**, *15*, 2868. [CrossRef]
22. Panagos, P.; Matthews, F.; Patault, E.; De Michele, C.; Quaranta, E.; Bezak, N.; Kaffas, K.; Patro, E.R.; Auel, C.; Schleiss, A.J.; et al. Understanding the cost of soil erosion: An assessment of the sediment removal costs from the reservoirs of the European Union. *J. Clean. Prod.* **2024**, *434*, 140183. [CrossRef]
23. Wischmeier, W.H.; Smith, D.D. Predicting rainfall erosion losses. *Agric. Handb.* **1978**, *537*, 285–291. [CrossRef]
24. Renard, K.; Foster, G.; Weesies, G.; McCool, D.; Yoder, D. *Predicting Soil Erosion by Water: A Guide to Conservation Planning with the Revised Universal Soil Loss Equation (RUSLE)*; Agricultural Handbook Number 703; US Department of Agriculture, Agricultural Research Service: Washington, DC, USA, 1997.
25. Arnold, J.G.; Moriasi, D.N.; Gassman, P.W.; Abbaspour, K.C.; White, M.J.; Srinivasan, R.; Santhi, C.; Harmel, R.D.; van Griensven, A.; Van Liew, M.W.; et al. SWAT: Model Use, Calibration, and Validation. *Trans. ASABE* **2012**, *55*, 1491–1508. [CrossRef]
26. Hydrologic Engineering Center HEC-RAS, River Analysis System, User's Manual, CPD-68, U.S. Army Corps of Engineers, Davis, CA, USA. Available online: http://www.hec.usace.army.mil/software/hec-ras/documentation/HEC-RAS%205.0%20Users%20Manual.pdf (accessed on 25 September 2024).
27. Flanagan, D.C.; Ascough, J.C.; Nearing, M.A.; Laflen, J.M. The Water Erosion Prediction Project (WEPP) Model. In *Landscape Erosion and Evolution Modeling*; Harmon, R.S., Doe, W.W., Eds.; Springer: Boston, MA, USA, 2001.
28. Bladé, E.; Cea, L.; Corestein, G.; Escolano, E.; Puertas, J.; Vázquez-Cendón, J.; Dolz, J.; Coll, A. IBER: Herramienta de simulación numérica de flujo en ríos. *Rev. Int. Métodos Numéricos Para Cálculo Diseño Ing.* **2014**, *30*, 1–10. [CrossRef]
29. López Reyes, M. Degradación de suelos en Sonora: El problema de la erosión en los suelos de uso ganadero. *Región Soc.* **2001**, *13*, 73–97. [CrossRef]
30. Muñoz-Arriola, F.; Avissar, R.; Zhu, C.; Lettenmaier, D.P. Sensitivity of the water resources of Rio Yaqui Basin, Mexico, to agriculture extensification under multiscale climate conditions. *Water Resour. Res.* **2009**, *45*, W00A20. [CrossRef]
31. Schoups, G.; Addams, L.; Battisti, D.S.; McCullough, E.; Minjares, J.L. Water Resources Management in the Yaqui Valley. In *Seeds of Sustainability*; Matson, P.A., Ed.; Island Press/Center for Resource Economics: Washington, DC, USA, 2012. [CrossRef]
32. Meza-Montenegro, M.M.; Valenzuela-Quintanar, A.I.; Balderas-Cortés, J.J.; Yañez-Estrada, L.; Gutiérrez-Coronado, M.L.; Cuevas-Robles, A.; Gandolfi, A.J. Exposure Assessment of Organochlorine Pesticides, Arsenic, and Lead in Children from the Major Agricultural Areas in Sonora, Mexico. *Arch. Environ. Contam. Toxicol.* **2013**, *64*, 519–527. [CrossRef]
33. Arreola-Lizarraga, J.; Garatuza-Payan, J.; Yepez, E.; Robles-Morua, A. Capital Natural y Bienestar Social de la Comunidad Yaqui. 2019. Available online: https://www.itson.mx/publicaciones/Documents/rec-nat/Capital%20natural%20y%20bienestar%20social%20de%20la%20comunidad%20Yaqui%20VF.pdf (accessed on 25 September 2024).
34. Vega-Granillo, E.L.; Cirett-Galán, S.; De la Parra-Velasco, M.L.; Zavala-Juárez, R. Hidrogeología de Sonora, México. In *Panorama de la Geología de Sonora, México*; Thierry, C., Ed.; Instituto de Geología, Universidad Nacional Autónoma de México: Ciudad de México, Mexico, 2011; pp. 267–298.

35. Portal de Geoinformación Sistema Nacional de Información Sobre Biodiversidad (SNIB). Available online: http://www.conabio.gob.mx/informacion/gis/ (accessed on 25 September 2024).
36. Corine Land Cover. Available online: https://land.copernicus.eu/en/products/corine-land-cover (accessed on 25 September 2024).
37. Landsat/Copernicus Satellites. Yaqui River Sub-Basin (Mexico). [Satellites Images]. Google Earth. Available online: https://earth.google.com/ (accessed on 25 September 2024).
38. Meyer-Peter, E.; Müller, R. Formulas for bedload transport. In Proceedings of the 2nd Congress, IAHR, Stockholm, Sweden, 7–9 June 1948.
39. Wong, M. Does the Bedload Equation of Meyer-Peter and Muller Fit Its Own Data? In *Proceedings of the 30th IAHR World Congress*; International Association of Hydraulic Research: Thessaloniki, Greece, 2003.
40. Wong, M.; Parker, G. Reanalysis and Correction of Bed-Load Relation of Meyer-Peter and Muller Using Their Own Database. *J. Hydraul. Eng.* **2006**, *132*, 1159–1168. [CrossRef]
41. Cea, L.; Legout, C.; Grangeon, T.; Nord, G. Impact of model simplifications on soil erosion predictions: Application of the GLUE methodology to a distributed event-based model at the hillslope scale. *Hydrol. Process.* **2016**, *30*, 1096–1113. [CrossRef]
42. Areu-Rangel, O.S.; Bonasia, R.; Di Traglia, F.; Del Soldato, M.; Casagli, N. Flood Susceptibility and Sediment Transport Analysis of Stromboli Island after the 3 July 2019 Paroxysmal Explosion. *Sustainability* **2020**, *12*, 3268. [CrossRef]
43. Bonasia, R.; Turchi, A.; Madonia, P.; Fornaciai, A.; Favalli, M.; Gioia, A.; Di Traglia, F. Modelling Erosion and Floods in Volcanic Environment: The Case Study of the Island of Vulcano (Aeolian Archipelago, Italy). *Sustainability* **2022**, *14*, 16549. [CrossRef]
44. Costabile, P.; Cea, L.; Barbaro, G.; Costanzo, C.; Llena, M.; Vericat, D. Evaluation of 2D hydrodynamic-based rainfall/runoff modelling for soil erosion assessment at a seasonal scale. *J. Hydrol.* **2024**, *632*, 130778. [CrossRef]
45. Fryrs, K.A.; Brielrey, G.J. *Geomorphic Analysis of River Systems: An Approach to Reading the Landscape*; John Wiley & Sons: Hoboken, NJ, USA, 2012. [CrossRef]
46. Knighton, D. *Fluvial Forms and Processes: A New Perspective*, 2nd ed.; Routledge: London, UK, 1998. [CrossRef]
47. Selby, M.J. *Hillslope Materials and Processes*, 2nd ed.; Oxford University Press: Oxford, UK, 1993.
48. Continuo de Elevaciones Mexicano. Available online: https://www.inegi.org.mx/app/geo2/elevacionesmex/ (accessed on 25 September 2024).
49. Isoyetas de Intensidad–Duración–Periodo de Retorno Para la República Mexicana. Available online: https://www.sct.gob.mx/carreteras/direccion-general-de-servicios-tecnicos/isoyetas/ (accessed on 25 September 2024).
50. Manifestación Impacto Ambiental. Available online: https://apps1.semarnat.gob.mx:8443/dgiraDocs/documentos/son/estudios/2023/26SO2023MD022.pdf (accessed on 25 September 2024).
51. Soulis, K.X. Soil Conservation Service Curve Number (SCS-CN) Method: Current Applications, Remaining Challenges, and Future Perspectives. *Water* **2021**, *13*, 192. [CrossRef]
52. de Alcántara, C.H. *La Modernización de la Agricultura Mexicana, 1940–1970*; Universidad de Texas: Austin, TX, USA, 1978.
53. Sonnenfeld, D. Mexico's "Green Revolution", 1940–1980: Towards an Environmental History. *Environ. Hist. Rev.* **1992**, *16*, 28–52. [CrossRef]
54. McCully, P. *Silenced Rivers: The Ecology and Politics of Large Dams*; Zed Books: London, UK, 2001.
55. Galindo, A.; Hopkins, J. Ryo Yaqui-The Hiak Vatwe: The transformation of a cultural landscape. In *Open Rivers: Rethinking Water, Place & Community*; Nunnally, P., Ed.; Open Rivers; University of Minnesota: Minneapolis, MN, USA, 2017.
56. Parsons, A.J. How reliable are our methods for estimating soil erosion by water? *Sci. Total Environ.* **2019**, *676*, 215–221. [CrossRef]
57. Evans, R.; Collins, A.L.; Foster, I.D.L.; Rickson, R.J.; Anthony, S.G.; Brewer, T.; Deeks, L.; Newell-Price, J.P.; Truckell, I.G.; Zhang, Y. Extent, frequency and rate of water erosion of arable land in Britain–benefits and challenges for modelling. *Soil Use Manag.* **2016**, *32*, 149–161. [CrossRef]
58. Kumar, N.; Singh, S.K.; Reddy Obi, G.P.; Mishra, V.N.; Bajpai, R.K. Remote Sensing and Geographic Information System in Water Erosion Assessment. *Agric. Rev.* **2020**, *41*, 116–123. [CrossRef]
59. Duressa, A.A.; Feyissa, T.A.; Tukura, N.B.; Gudeta, B.G.; Gechelu, G.F.; Bibi, T.S. Identification of soil erosion-prone areas for effective mitigation measures using a combined approach of morphometric analysis and geographical information system. *Results Eng.* **2024**, *21*, 101712. [CrossRef]
60. Bressan, F.; Mantilla, R.; Schilling, K.E.; Palmer, J.A.; Weber, L. Hydrologic-hydraulic modeling of sediment transport along the main stem of a watershed: Role of tributaries and channel geometry. *Hydrol. Sci. J.* **2019**, *65*, 183–199. [CrossRef]
61. Tu, T.; Ercan, A.; Carr, K.J.; Kavvas, L.M.; Trinh, T.; Ishida, K.; Nosacka, J.; Brown, K. Coupling hydroclimate-hydraulic-sedimentation models to estimate flood inundation and sediment transport during extreme flood events under a changing climate. *Sci. Total Environ.* **2020**, *740*, 140117. [CrossRef]

Disclaimer/Publisher's Note: The statements, opinions and data contained in all publications are solely those of the individual author(s) and contributor(s) and not of MDPI and/or the editor(s). MDPI and/or the editor(s) disclaim responsibility for any injury to people or property resulting from any ideas, methods, instructions or products referred to in the content.